



RESEARCH ARTICLE

10.1002/2015JB012253

Key Points:

- A correlation-weighted spatial filtering is developed for CGPS data analysis
- The filter achieves significant common-mode signal reduction
- The filter can extract any signals common to a subset of a CGPS network

Supporting Information:

- Figures S1–S6

Correspondence to:

Z.-K. Shen,
zshen@ucla.edu

Citation:

Tian, Y., and Z.-K. Shen (2016), Extracting the regional common-mode component of GPS station position time series from dense continuous network, *J. Geophys. Res. Solid Earth*, 121, doi:10.1002/2015JB012253.

Received 4 JUN 2015

Accepted 3 JAN 2016

Accepted article online 7 JAN 2016

Extracting the regional common-mode component of GPS station position time series from dense continuous network

Yunfeng Tian¹ and Zheng-Kang Shen^{2,3}

¹Key Laboratory of Crustal Dynamics, Institute of Crustal Dynamics, China Earthquake Administration, Beijing, China,

²School of Earth and Space Sciences, Peking University, Beijing, China, ³Department of Earth, Planetary, and Space Sciences, University of California, Los Angeles, California, USA

Abstract We develop a spatial filtering method to remove random noise and extract the spatially correlated transients (i.e., common-mode component (CMC)) that deviate from zero mean over the span of detrended position time series of a continuous Global Positioning System (CGPS) network. The technique utilizes a weighting scheme that incorporates two factors—distances between neighboring sites and their correlations of long-term residual position time series. We use a grid search algorithm to find the optimal thresholds for deriving the CMC that minimizes the root-mean-square (RMS) of the filtered residual position time series. Comparing to the principal component analysis technique, our method achieves better (>13% on average) reduction of residual position scatters for the CGPS stations in western North America, eliminating regional transients of all spatial scales. It also has advantages in data manipulation: less intervention and applicable to a dense network of any spatial extent. Our method can also be used to detect CMC irrespective of its origins (i.e., tectonic or nontectonic), if such signals are of particular interests for further study. By varying the filtering distance range, the long-range CMC related to atmospheric disturbance can be filtered out, uncovering CMC associated with transient tectonic deformation. A correlation-based clustering algorithm is adopted to identify stations cluster that share the common regional transient characteristics.

1. Introduction

The Global Positioning System (GPS) technique has been used for broad purposes on earthquake and tectonic studies, such as investigations of regional tectonic deformation [e.g., Mazzotti *et al.*, 2003; Meade and Hager, 2005; Calais *et al.*, 2006; Takayama and Yoshida, 2007; Shen *et al.*, 2011], coseismic displacements and earthquake rupture [e.g., Melbourne *et al.*, 2002; Freed *et al.*, 2006; Barbot *et al.*, 2009; Savage and Langbein, 2008; Savage and Svarc, 2009], slow slip events [e.g., Szeliga *et al.*, 2004; Melbourne *et al.*, 2005; Heki and Kataoka, 2008; Brooks *et al.*, 2008; Wech *et al.*, 2009; Holtkamp and Brudzinski, 2010; Fu and Freymueller, 2013; Schmalzle *et al.*, 2014], global plate motion [e.g., Prawirodirdjo and Bock, 2004; Kogan and Steblov, 2008], and postglacial rebound [e.g., Sella *et al.*, 2007; Khan *et al.*, 2008]. It has been the focus in the past two decades to improve GPS positioning accuracy for detection of more subtle deformation signals [e.g., Wdowinski *et al.*, 1997; Dong *et al.*, 2006]. Some recent studies on the subject have been on filtering of the continuous GPS (CGPS) data and detecting transient deformation signals; the latter is profoundly important in understanding the tectonic processes of fault zone system and earthquake dynamics [e.g., Ji and Herring, 2011].

CGPS positions derived under the International Terrestrial Reference Frame usually suffer from spatial-temporal correlated noises, making it challenging to discern subtle tectonic signals from data. In addition, GPS results usually include displacement signals from other geophysical processes and/or human activities. Efforts have been made to suppress the noise in the data and explore the tectonic deformation sources. It was found, for example, that a portion of position scatters and most of seasonal motions can be attributed to loading effects caused by Earth surface and subsurface mass redistributions [e.g., vanDam *et al.*, 1994; Dong *et al.*, 2002; Argus *et al.*, 2005; Tregoning and van Dam, 2005; Amos *et al.*, 2014; Borsa *et al.*, 2014]. After removing a linear trend, annual and semiannual terms, jumps, and postseismic decays in CGPS position time series, the most prominent feature in position residuals is the common-mode error (CME) which results from unmodeled or mismodeled effects during data processing [e.g., Wdowinski *et al.*, 1997; Nikolaidis, 2002; Dong *et al.*, 2006]. Beside CME, other types of (tectonic or nontectonic) activities can also produce regional motion of CGPS stations, e.g., surface displacements caused by aseismic episodic tremor and slip (ETS) events on faults, volcanic inflation/deflation

©2016. The Authors.

This is an open access article under the terms of the Creative Commons Attribution-NonCommercial-NoDerivs License, which permits use and distribution in any medium, provided the original work is properly cited, the use is non-commercial and no modifications or adaptations are made.

[e.g., Webb *et al.*, 1995; Dragert *et al.*, 2001; Larson *et al.*, 2010], or underground water recharging [e.g., King *et al.*, 2007]. Because common-mode position shifts are usually estimated through statistical means and may consist not only errors but also signals (depending on the subjects of research), we use a slightly different term of common-mode component (CMC) for them. For tectonic studies, the large-scale CMC equals the traditional CME.

Two methods are often used to remove CME: spatial filtering of residual positions [Wdowski *et al.*, 1997; Nikolaidis, 2002; Dong *et al.*, 2006] and constraining the solution to a regional reference frame [Szeliga *et al.*, 2004; Melbourne *et al.*, 2005]. These techniques facilitate better detection of transient slip events and have been widely used in geodetic studies [e.g., Lin *et al.*, 2010; Ji and Herring, 2012; Jiang *et al.*, 2012; Marshall *et al.*, 2013; Blewitt *et al.*, 2013]. Current methods, however, have certain limitations dealing with CMC. For regional stacking filtering method [e.g., Nikolaidis, 2002], it works well only when CME is nearly spatially homogenous in a network. The common part of fluctuations in position residuals of sites nevertheless decreases with increased spatial separation [Márquez-Azúa and Demets, 2003; Williams *et al.*, 2004]. For the Plate Boundary Observatory (PBO) network whose extent exceeds 2000 km, there are remarkable differences in CMC in various areas. The Scripps Orbit and Permanent Array Center (SOPAC) therefore divided the whole network into several subregions of 400–1000 km in size and performed stacking filtering individually (<http://sopac.ucsd.edu>). However, the division of subregions is somewhat arbitrary. This strategy also requires specifying a few base stations, and problems may occur if some of them endure regional deformation themselves. As for the principal component analysis (PCA) and Karhunen-Loeve expansion (KLE) techniques [Dong *et al.*, 2006], the derived results often need further visual work and subtle regional transient signals may not appear in the first several principal components when there are strong local effects (which is true in most cases). In the case of using a regional reference frame, there might be distorted signals for stations located at the network edge when the network is too wide, and at the same time, the seasonal motion and vertical trend estimations are often biased.

With the fast expansion of CGPS networks, we are facing a challenge to find an optimal and objective method to extract CMC without consideration of spatial extent of the CGPS network, and it can be used to extract spatial and temporal characteristics of certain signals if necessary. Attempts have been made in this regard among some of previous studies. In order to remove CME for CGPS stations across the North American plate, Márquez-Azúa and Demets [2003] adopted the lengths of time series and baselines as weights when applying stacking filtering. They used a simplified correlation weighting scheme in which the relationship between baseline length and correlation was assumed to decrease linearly from one to zero when the baseline length increases from 500 km to 2000 km, which is a rough approximation of reality and ignores its local and regional variations. Williams *et al.* [2004] also found that correlation decreases as station separation increases. However, they used a weighted mean of correlation results, and the stacked correlation-baseline length curve may not reveal the trend accurately, because correlation level can deviate from the trend greatly at locations, and thus, the stacked curve could be biased.

In this paper, we attempt to characterize the spatial variations of CMC more accurately by investigating correlations between long-term residual position time series of CGPS stations. We then put forward a correlation-based spatial filtering method to extract CMC and use that to filter the data. This method is further tuned so that it can optimally extract the CMC associated with certain regional deformation signals.

2. Data

The CGPS station position time series used in this paper are obtained from SOPAC GPS data analysis. The cleaned residual position time series for the western North America (WNAM) network (ftp://garner.ucsd.edu/pub/timeseries/measures/ats/WesternNorthAmerica/WNAM_Clean_ResidNeuTimeSeries_comb_20150318.tar) are used as raw data input, which consist of data for 1659 CGPS sites (Figure 1). SOPAC has already removed the long-term linear trend, annual and semiannual sinusoid variations, coseismic and instrument jumps, and logarithmic post-seismic displacements for a number of strong earthquakes. Data outliers are also cleaned from the time series. The filtered residual position time series derived using PCA [Dong *et al.*, 2006] technique (ftp://garner.ucsd.edu/pub/timeseries/measures/ats/WesternNorthAmerica/WNAM_Filter_ResidNeuTimeSeries_comb_20150318.tar), which consist of the filtered data for 1639 stations, are used for comparison. For details of modeling and removal of these terms, the readers may refer to SOPAC website links (e.g., ftp://garner.ucsd.edu/pub/timeseries/measures/ats/ATS_TarFile_README.txt).

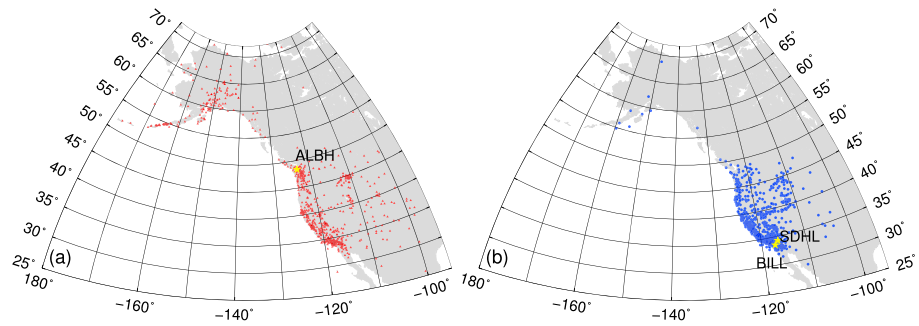


Figure 1. Locations of WNAM CGPS stations. (a) Red triangles are transient (Group I) sites defined in section 3.2; (b) blue dots represent steady (Group II) sites. The yellow stars show locations of sites ALBH, BILL, and SDHL.

3. Position Similarity in CGPS Network Data Set

3.1. Representation of Interstation Positions Similarity

We use Lin's concordance correlation coefficient [Lin, 1989, 2000] to represent the similarity of residual position time series between two CGPS sites. It is calculated for each component as

$$r_{xy} = \frac{\frac{2}{N} \sum_{k=1}^N (x_k - \bar{x})(y_k - \bar{y})}{\frac{1}{N} \sum_{k=1}^N (x_k - \bar{x})^2 + \frac{1}{N} \sum_{k=1}^N (y_k - \bar{y})^2 + (\bar{x} - \bar{y})^2} \quad (1)$$

where x and y are the residual time series, \bar{x} and \bar{y} are the means of time series (both are zero in this case), N is the number of common days in which both sites have data records, and r_{xy} is the concordance correlation coefficient. Difference between concordance correlation and classic Pearson correlation is that this form of correlation takes into account similarities of not only the shapes but also amplitudes of two time series.

3.2. Correlation Analysis of WNAM CGPS Network

Time series correlation analysis results for all 1659 WNAM CGPS stations show that the interstation correlation is approximately inversely proportional to site separation range (radial distance). The correlation between two stable adjacent sites can be strong; e.g., correlation coefficient of the north components between BALD and KRAC stations (in Mammoth Lakes, California; about 8 km apart; and both are enduring similar large nonlinear movements) is 0.96 for the total time span.

As pointed out in section 1, many sites in this data set are affected by various kinds of local nonlinear motions, such as ETS events in the Cascadia subduction zone. The far-field interstation correlations associated with these sites are rather low since they do not share the same transients. To analyze the characteristic of large-scale CMC (the traditional CME), these factors should be excluded first. We here use a residual root-mean-square (RMS) threshold to separate the whole network into two groups: transient sites (Group I) whose time series contain obvious nonlinear motions which may result from known nontectonic factors (e.g., underground water level variations), slow slip, and/or volcanic activities; and steady stations (Group II) with small residual scatters. Among the 1639 PCA-filtered sites, the ones whose residual RMS belong to the lower 60% portion of statistics (for all three components) are classified into Group II, which amounts to a total number of 751 sites (Figure 1b). The use of filtered time series for site grouping highlights the effect of regional transients or site-specified abnormal motions, at the same time suppressing the effect of CME. It is noted that this distinction may not work very well for regions with sparse site population, where more stations are categorized in Group I than in Group II. This, however, should not have significant effect on our analysis since this study focuses mainly on networks with dense population.

Correlations are usually high among sites affected by regional transients and low between sites located inside and outside of the region. The linear decreasing trend in correlation-baseline length relationship is therefore more prominent when just using those relatively stable stations in Group II in the analysis. One typical result is shown in Figure 2 for site BILL whose geographic location is shown in Figure 1b.

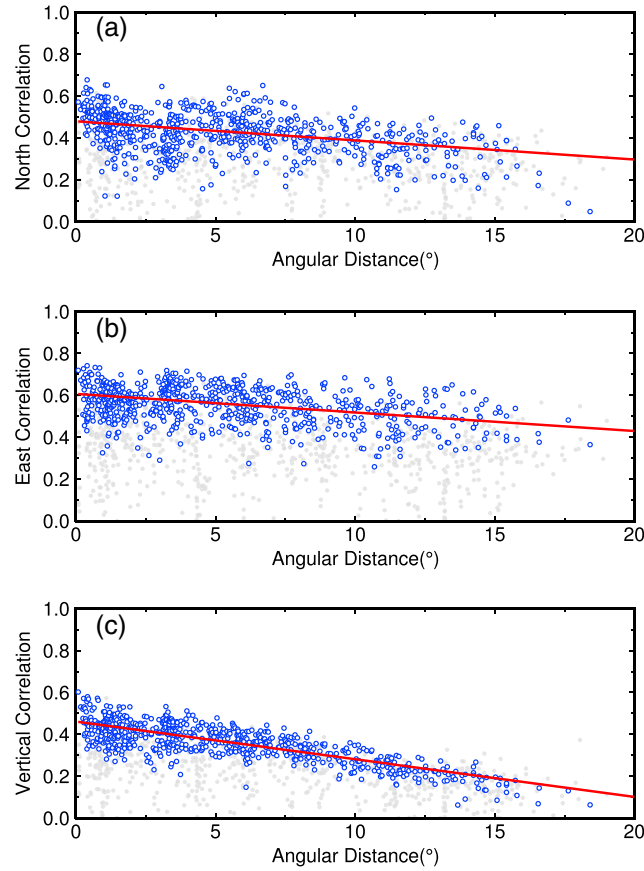


Figure 2. Residual station position correlations between BILL and other sites. The X axes denote the radial distance in degrees (only sites within 20° arc distance are shown in the plots), and the Y axes are the correlation coefficients for the (a) north, (b) east, and (c) vertical components, respectively. The blue circles are raw data derived using only those steady CGPS stations (Group II), and the red lines show their linear fits using a robust least absolute deviation technique [William *et al.*, 1992] which is less sensitive to data outliers than the least squares method. The gray dots represent correlations between BILL and Group I stations.

For the i th and j th stations, r_{ij} is the correlation coefficient between residual position time series of the i th and j th stations, d_{ij} is the radial distance between the i th and j th stations, τ_i is a distance weighting constant to regulate weighting by distance between stations, w'_{ij} is the w_{ij} sequence sorted in descending order according to their values, and W_i is a parameter to be determined. A minimum number of stations required to derive CMC is usually set by the users, to make the result more robust. w_{ij} could be negative in theory, but W_i would not because of optimal selections of τ_i and w'_{ij} in equation (3).

Our method uses the calculated interstation correlation coefficients as the weights in the filtering process. Comparing to a different approach of using fitted correlation relation (red lines in Figure 2), our method incorporates all possible factors that contribute to the correlation. For example, correlations will be smaller for sites that are affected by small-scale or site-specific variations; and in such cases, our method will assign smaller weights to those sites than a spatial fitting scheme would do.

To optimally select sites in calculating CMC, we use a grid search of τ and W to determine the optimal threshold values of τ and W that produce the lowest RMS for the filtered residual position time series. For a given pair of τ and W , we compute weight w_{ij} as defined in equation (3) for each site pair i and j , which means, the higher the correlation is and the closer the site j is to site i , the larger w_{ij} becomes. We then sort w_{ij} to produce w'_{ij} and choose the first $N_{i,k}$ sites for CMC derivation, where $N_{i,k}$ is decided by the condition shown in equation (3) (the summation stops when the inequality no long holds).

4. Algorithm of Extracting CMC

The derivation of CMC in our Correlation-Weighted Spatial Filtering (CWSF) method is somewhat similar to traditional stacking techniques [e.g., *Wdowinski et al.*, 1997; *Nikolaïdis*, 2002; *Márquez-Azúa and Demets*, 2003] but differs in details. We deduce the CMC time series for each site by introducing a new weight factor (w_{ij} in equation (2)) and a grid search scheme (which ensures that optimal results will be obtained).

For the i th station on the k th day, the CMC $\varepsilon_{i,k}$ is calculated for each (east, north, or vertical) component separately as

$$\varepsilon_{i,k} = \frac{\sum_{j=1}^{N_{i,k}} v_{j,k} \times w_{ij}}{\sum_{j=1}^{N_{i,k}} \sigma_{j,k}^2 \times w_{ij}} \quad (2)$$

where $v_{j,k}$ and $\sigma_{j,k}$ are residual and formal error of the position for the j th station on the k th day, respectively, and $N_{i,k}$ is the number of sites used to derive CMC. The weight w_{ij} is calculated as

$$\left\{ \begin{array}{l} w_{ij} = r_{ij} \times \exp\left(-\frac{d_{ij}^2}{\tau_i^2}\right) \\ \sum_{j=1}^{N_{i,k}} w'_{ij} < W_i \end{array} \right. \quad (3)$$

where r_{ij} is the correlation coefficient between residual position time series of the i th and j th stations, d_{ij} is the radial

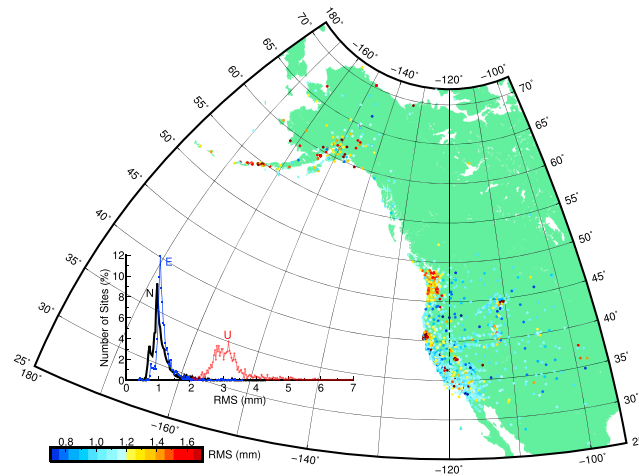


Figure 3. Amplitudes of the east CMC time series obtained using the CWSF filter. The color dots represent the RMS of the time series. The inset plot shows the RMS histograms for individual components: black = north (N), blue = east (E), and red = vertical (U).

have certain meanings. The parameter τ maps the extent of the most contributing wavelength to CMC. In many cases, the larger CMC amplitudes correspond with the occurrence of small τ values, which suggests the presence of regional transients at those locations. Also, regions with dense CGPS networks, such as the Los Angeles basin, tend to show more correlations among sites and smaller τ values.

We compare our filtered results with that produced by SOPAC using the PCA/KLE method. Our filtered positions gain a noticeable reduction in terms of residual RMS for all the three position components (Figure 5)—with mean improvements of 20.7%, 13.2%, and 14.4% for the north, east, and vertical components, respectively. The relative improvement also agrees well with the CMC map in Figure 3. Stations with largest improvements are located in a wide region surrounding the Cascadia subduction zone and some areas with dense networks along the Pacific coast. Comparing our result with that of the SOPAC PCA filtering, we find that all the detectable regional CMCs (e.g., ETS) have been eliminated in our filtered results, but not in the SOPAC PCA-filtered positions. Therefore, if the purpose is to eliminate regional transients, a remarkable improvement (e.g., > 20%) can be achieved in regions experiencing known transient processes. For most other WNAM CGPS stations without apparent transient events, we still achieve more than 5% RMS reductions over PCA results (as shown in the RMS reduction histograms in Figure 5). The additional reduction of residual scatters (especially for the Group II sites) achieved by using our filtering algorithm indicates the existence of detectable small-scale common-mode variations which the PCA technique might be inadequate to extract.

5.2. Extraction of Regional Transients

5.2.1. Algorithm of Identifying Transient Events

We employ a phenomenological analysis of the data to separate tectonic signals from noises. Since regional tectonic crustal deformations (e.g., episodic sawtooths caused by ETS events) are usually limited in a certain geographic range (e.g., tens of kilometers), it is possible to identify the existence of such a signal and locate its spatial extent with a dense CGPS network. To do so, we need to screen out the random noise and large-scale (hundreds of kilometers) CMC (mostly due to atmospheric disturbance) from the total CMC estimates. For a residual station position time series P , in the first step we obtain CMC_0 , which represents the spatially correlated term at all spatial ranges. Therefore, if we define noise as spatially random fluctuation of the time series, it is $P - CMC_0$; i.e., we have separated that part of noise. In the second step we evaluate CMC_D (the subscript D here indicates using sites beyond the arc distance of D° to derive CMC) and deduce $\Delta CMC = CMC_0 - CMC_D$. In doing so, we exclude the far-field CMC which is dominated by atmospheric disturbance effect and left with the regional CMC only. This portion of CMC is closely associated with various regional geophysical processes, which have the time scale of days to years and spatial scale of tens to hundreds of kilometers. For the interest on transient spatial wavelength, a series of stepwise distance thresholds D (e.g., let $D = 0^\circ, 0.5^\circ, 1^\circ, \dots$) can be attempted; the corresponding D across which the highest RMS gradient occurs represents the approximate spatial extent of the transient signal.

5. Application of CWSF to CGPS Network Data Filtering

5.1. Comparison of Results From CWSF and PCA

For the 1659 WNAM CGPS stations, the CMC time series are derived using our spatial filter (equations (2) and (3)) component by component. The searching ranges for parameters τ (in unit of angular degrees) and W are both set to vary from 1 to 50, with a step size of 5. The minimum number of stations ($N_{i,k}$) required to derive CMC is set to 3.

The geographic variation of the total amount of the resulting CMC (Figure 3) shows that there are several clusters with large CMC. The two free parameters τ and W in equation (3) (Figure 4) also

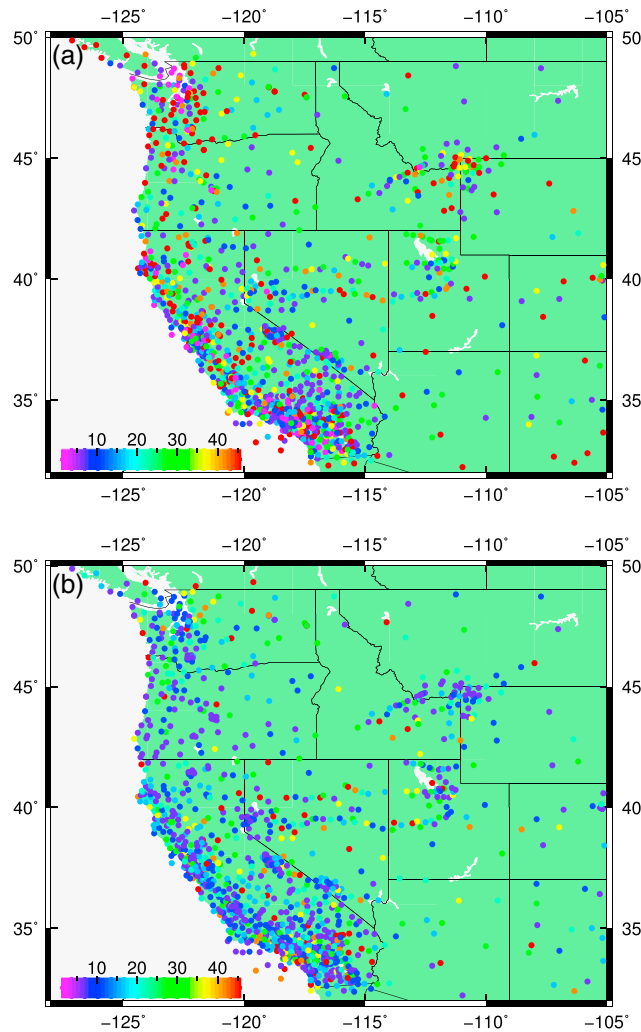


Figure 4. Optimal values of parameter (a) τ and (b) W in equation (3) adopted in the east CMC extraction for the WNAM network, obtained from grid search. Parameter τ is of the unit of radial degrees, and W has no unit.

with closest correlative distance are first linked together to form a parent node. Subsequent nodes are created by pairwise joining of other sites or nodes based on the subsequent closest correlative distances between them. There are several methods [de Hoon et al., 2004] to merge nodes/sites which are deemed to be closest. We adopt the single-linkage (nearest neighbor) method; i.e., the distance between two clusters (nodes) is defined as the shortest distance among all the pairwise distances between the members of the two clusters. At the final step all stations merge into one branch, a tree structure is then created by retracing the procedure following the routes the sites/nodes were merged. The key aspect of our spatial filtering method is the interstation correlations which are derived from existing residual station position time series. The correlation coefficients used in the filtering process are calculated using the overlapping time span between each site pair. Therefore, two sites having no common epochs can still be grouped together, as long as they are both highly correlated to a third station.

Finally, cutting the hierarchical tree at a given “height” of the correlative distance will produce a series of clusters which contain groups of stations affected by various regional transients. Each cluster is composed of a set of stations which belong to a subnode below the cutting line. A sample of derived hierarchical tree is shown in Figure S1 in the supporting information. It demonstrates that if the correlative distance $c=0.3$, five groups of sites are differentiated, each showing some regional characteristics.

The next task is to identify the spatial scope of (i.e., sites that are affected by) regional transients. We perform a hierarchical clustering [de Hoon et al., 2004] analysis, which had been used in several geodetic studies [e.g., Simpson et al., 2012; Savage and Simpson, 2013], to find a group of sites that are affected by an individual transient, based upon the Δ CMC time series. The first step in hierarchical clustering is to calculate the similarity matrix for all stations for each component of the Δ CMC time series as described in previous sections. The next is to use the correlations in the similarity matrix to deduce a “correlative distance” matrix, specifying the “distance measure” between the stations to be clustered. The correlative distance c for a site pair is defined as (http://www.exelisvis.com/docs/distance_measure.html)

$$c = \sqrt{\frac{(1-r)}{2}} \quad (4)$$

where r is the concordance correlation coefficient in the similarity matrix derived using equation (1). A greater correlative distance means less similarity between two sites.

Next, we rank the sites to form a hierarchical tree in an iterative way based upon the correlative distances between stations and nodes. The two stations

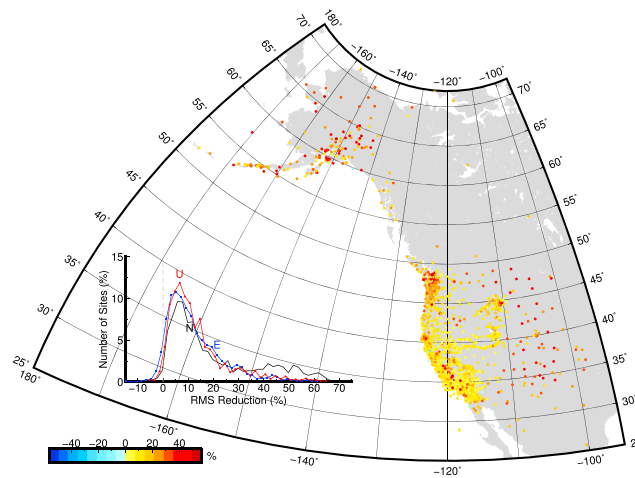


Figure 5. RMS improvements of CWSF over PCA filtering. The color-coded percentage represents the average improvement for three components. The inset plot shows the histograms of RMS improvements for individual components: black = north, blue = east, and red = vertical.

5.2.2. Extracting Regional Transients From WNAM CGPS Network

We extract regional transient signals from the WNAM CGPS stations by employing the strategy described in the previous section. We use the distance bound of $D=3.5^\circ$ to derive ΔCMC time series, because 3.5° is a reasonable distance range that is larger than the spatial scope of most regional CMCs and is still within the WNAM CGPS network extent. The value nevertheless could vary for other networks. For each one of the 1659 sites, the CMC_D ($D=0, 3.5$) time series are derived using the method described in section 5.1. We then calculate the difference of the two CMC time series as $\Delta\text{CMC} = \text{CMC}_{0-3.5} = \text{CMC}_0 - \text{CMC}_{3.5}$ which serves as the basis for detecting regional transient signals later.

The procedure of detecting transients can be examined by the variations of time series spectra. The spectrum of the raw time series includes various ingredients, such as regional tectonic deformation, local or regional hydrological disturbance, regional- or large-scale atmospheric disturbance, local site disturbance, and other noise due to errors in GPS measurements and data processing (e.g., orbital error, reference frame error, and multipath effect). These ingredients have somewhat different spatial and temporal patterns and therefore can be differentiated through filtering. The differential CMC time series (ΔCMC) is supposed to contain only regional transient signals. Figure 6 presents the filtering effect on power spectrum for the east component of station ALBH whose motions are affected by Cascadia ETS events. The raw time series spectrum (Figure 6a) shows colored noise plus white noise, consistent with previous findings [e.g., Zhang *et al.*, 1997; Williams *et al.*, 2004]. The first filtering results are shown in Figures 6b and 6c, which are the spectra of CMC_0 and the filtered residual time series after subtraction of CMC_0 contributions (i.e., FLT_0), respectively. Comparing to the raw time series, CMC_0 spectrum is more colored and FLT_0 is more white, reflecting somewhat different deformation patterns of the ingredients. The most prominent tectonic deformation signal is the ETS showing as the low-frequency peak at $\sim 2.7 \times 10^{-8}$ in Figures 6a and 6b. This signal, however, is much reduced in FLT_0 . Other geophysical signals such as hydrological disturbances are regional phenomena with relatively lower frequency and are mostly reflected in CMC_0 but not in FLT_0 . The GPS data measurement and processing errors are partially reflected in the higher-frequency components in CMC_0 . Some of the low-frequency components in FLT_0 may reflect individual site disturbances. The $\text{CMC}_{3.5}$ (Figure 6d) is obtained using only data from far-field sites. It is similar to CMC_0 except that the lower frequency signals are much reduced. This is because transient tectonic deformation such as due to the ETS events is mostly regional and not reflected in the far-field correlations. It therefore mostly reflects the large-scale coherent noise due to atmospheric disturbance and errors related to GPS measurement and data processing such as reference frame and orbital errors. The filtered time series by subtracting $\text{CMC}_{3.5}$ from the raw (i.e., $\text{FLT}_{3.5}$; Figure 6e) keeps the rest of the ingredients except the large-scale coherent noise shown in $\text{CMC}_{3.5}$. Figure 6f shows the spectrum of ΔCMC , which is the differential coherent signal between all scale coherency and large-scale coherency, left with the regional coherent signal only, clearly seen in the spectrum of lower frequency. The higher-frequency components are much reduced comparing to that in CMC_0 , suggesting that high-frequency noise related to large-scale atmospheric disturbance and orbital and reference frame errors are removed. Such assessments are supported in Figure S2 in the supporting information, which shows that the ΔCMC of site ALBH can be differentiated into higher and lower frequency components; the low-frequency part is dominated by ETS events (Figure S2a), and the higher-frequency part is dominated by other regional geophysical processes and noise (Figure S2b), whose spatial correlations decrease sharply with site separation distance (Figure S2c).

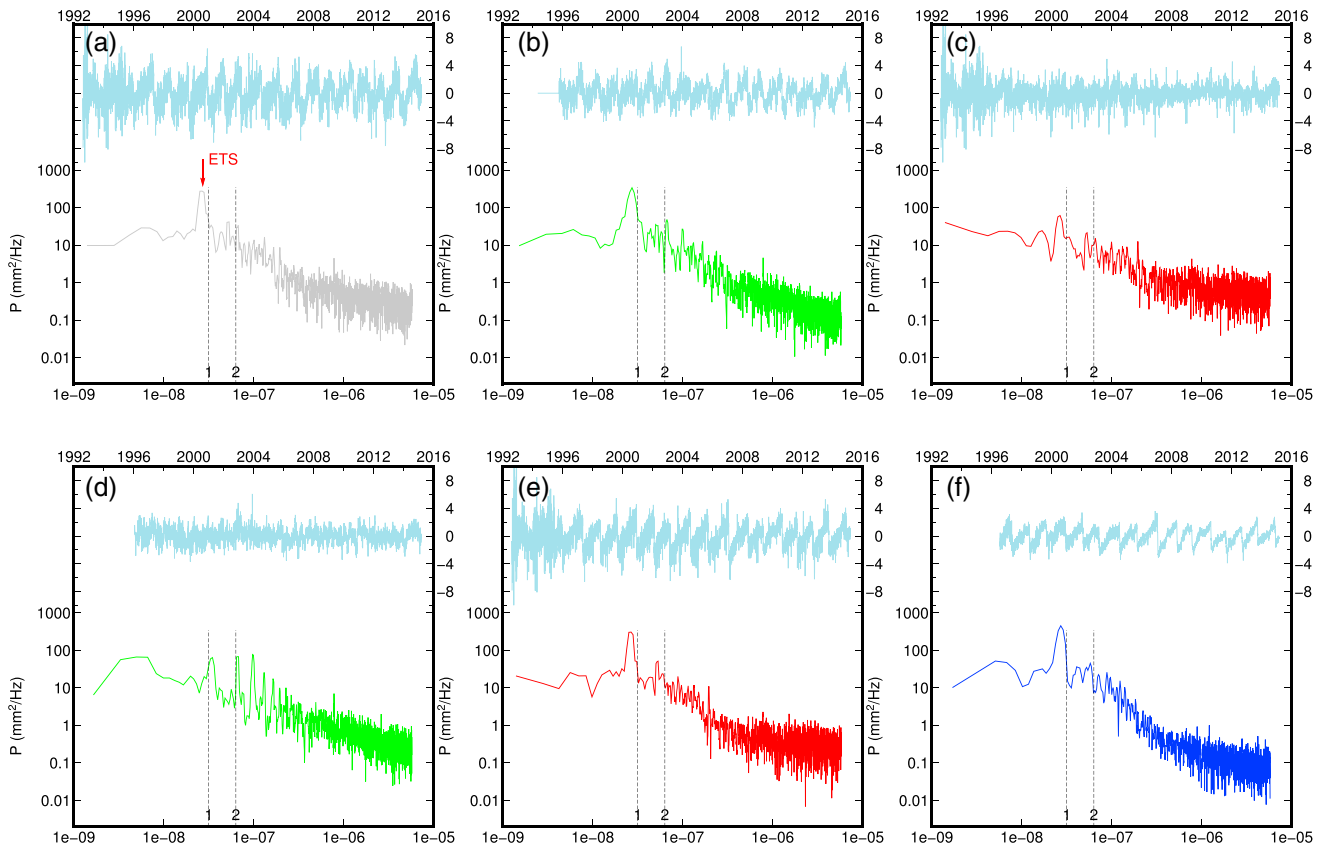


Figure 6. Spectra for the east component of station ALBH. (a) The raw time series; (b) CMC_0 ; (c) FLT_0 , the filtered time series after subtraction of CMC_0 contributions; (d) $CMC_{3.5}$; (e) $FLT_{3.5}$, the filtered time series by subtracting $CMC_{3.5}$; (f) ΔCMC . In each plot, the upper is position time series (in mm) and the lower is the spectrum. The raw spectral curves are smoothed with a boxcar filter of 0.01 cpy (cycles per year) width. The arrow in Figure 6a points to the frequency peak of Cascadia ETS events. The vertical dashed lines indicate harmonics of 1 cpy.

The filtering effects on spectra for steady sites are somewhat different. For example, for site SDHL (belongs to Group II), the most noticeable signals are the anomalous harmonics [e.g., Ray et al., 2008] near 1 cpy and 2 cpy which are almost eliminated in FLT_0 and greatly reduced in $FLT_{3.5}$ (Figure S3 in the supporting information). The amplitudes of all WNAM CGPS ΔCMC time series are shown in Figure 7 which agrees well with the spatial distribution of CMC map (Figure 3), but with improved spatial coherency.

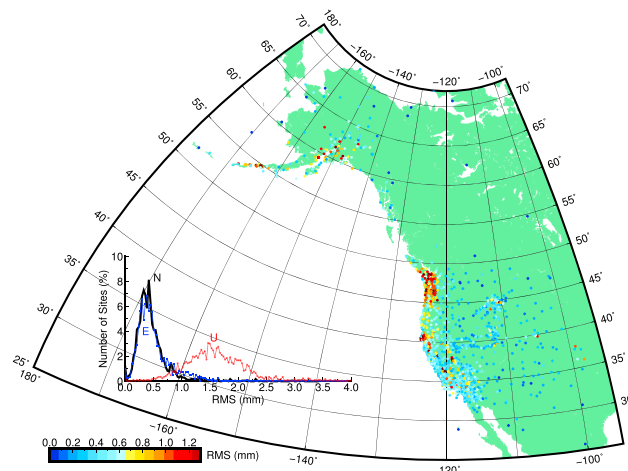


Figure 7. Amplitudes of the east ΔCMC time series for WNAM CGPS stations. The plot specifications are similar to those in Figure 3.

For each position component, a correlation matrix is derived for all the sites using the ΔCMC time series as the input, followed by a hierarchical clustering analysis. We use a cutting correlative distance of 0.3 to form the site clusters. The minimum number of members in each cluster is set to 2, in order to capture all the small-scale transients. These clusters are then sorted according to the number of member sites in each cluster. For the east component, we finally obtained 45 clusters. We first present the results for seven clusters which have at least nine member sites as shown in Figure 8.

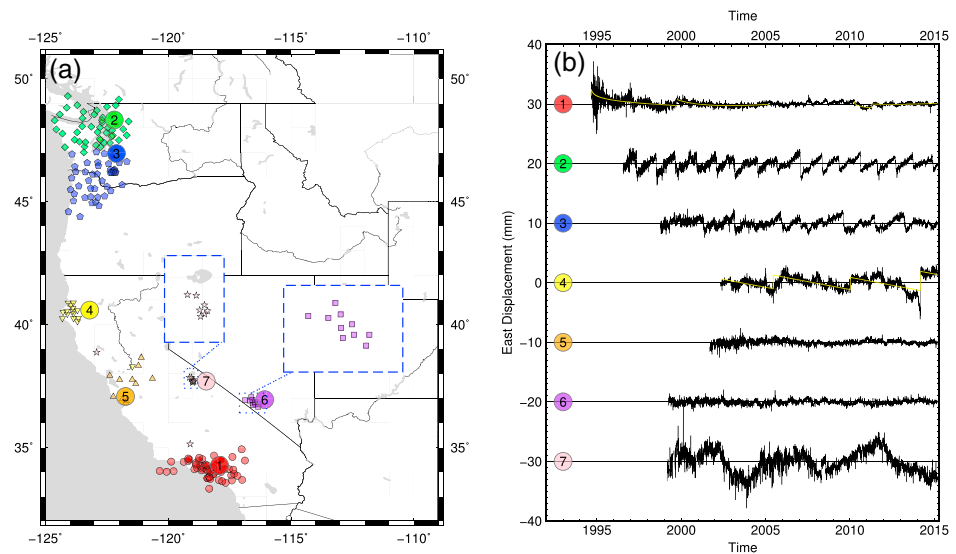


Figure 8. Regional transient clusters for the east component (only clusters with greater than or equal to nine member sites are presented here). (a) Map view of the clusters, shown as groups of colored symbols. (b) The mean Δ CMC time series for numbered clusters. The yellow curves in Δ CMC time series plots are modeled position jumps or logarithmic postseismic decays.

The first cluster reveals a few weak regional transient signals for CGPS sites in Los Angeles area and several offshore islands, California: (a) a logarithmic-like postseismic decay following the 17 January 1994 M_w 6.7 Northridge earthquake; (b) larger scatters resulting from poor realization of reference frame with only sparse fiducial stations in the 1990s; (c) uncorrected postseismic deformations following the 16 October 1999 M_w 7.1 Hector Mine earthquake; (d) the uncorrected post seismic displacements following the 4 April 2010 M_w 7.2 El Mayor-Cucapah earthquake at a portion of member stations (those situated at the northwest corner of the cluster); and (e) one nontectonic jump occurred on 17 April 2011 which was possibly a solution error but not completely removed during the time series analysis (noticeable at CBHS, CIRX, COPR, CRU1, CSN1, CSST, CTDM, FMVT, HVYS, LAPC, LEEP, LFRS, MIG1, MPWD, PVRS, SRS1, VNCX, and WMAP).

Two regions affected by evident ETS events are identified: the second cluster with 49 CGPS sites in northern Cascadia subduction zone [e.g., *Szeliga et al.*, 2004] and the third cluster with 45 stations in central Cascadia [e.g., *Holtkamp and Brudzinski*, 2010].

The fourth cluster sites reveal seismic displacements caused by several Mendocino Triple Junction (MTJ) offshore earthquakes: (a) the 15 June 2005 M_w 7.2 quake off the coast of Northern California (http://earthquake.usgs.gov/earthquakes/eventpage/iscgem7143782#general_summary), (b) the 10 January 2010 M 6.5 offshore Northern California earthquake (http://earthquake.usgs.gov/earthquakes/eventpage/usp000h5we#general_summary) [e.g., *Wei and McGuire*, 2014], and (c) the 10 March 2014 M_w 6.8 offshore earthquake, 77 km WNW of Ferndale, California (http://earthquake.usgs.gov/earthquakes/eventpage/nc72182046#general_summary).

The fifth and sixth clusters in Figure 8 reveal certain subtle irregular fluctuations of positions for regional CGPS stations whose origins are not so obvious. The seventh cluster represents the long term volcanic activities around the Long Valley Caldera, California [e.g., *Ji et al.*, 2013].

Our transient detector also identified a few small-scale coherent signals (limited to two to eight sites in the above clustering), and the results are presented in Figure 9 and Table A1 in Appendix A. Some of those are originated from the same sources as the transients shown in Figure 8. For example, the thirteenth, 29th, and 32nd clusters are partially similar to the fourth cluster; and the tenth, eleventh, fourteenth, and 26th clusters show very weak residual postseismic deformations due to the 4 April 2010 M_w 7.2 El Mayor-Cucapah earthquake.

In addition to those well-known transients, our approach also obtains more cases of certain interesting signals. For example,

1. CGPS stations in two places of California (the 37th cluster for Mono Lake; the 39th cluster for Searles Lake) show prominent skewed position scatters (i.e., larger scatters in only certain particular orientation), which

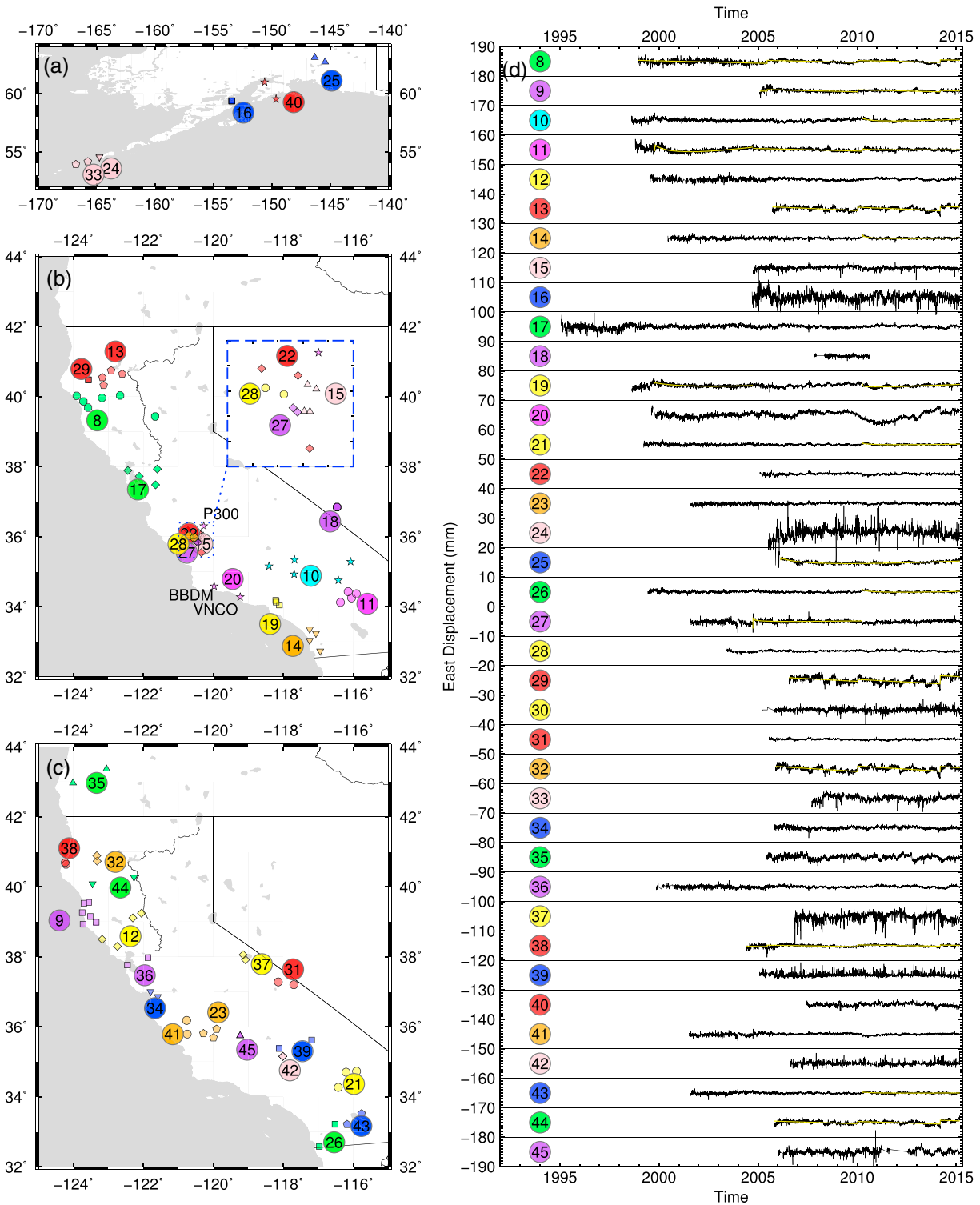


Figure 9. Same as Figure 8, but for transient clusters with less than nine member sites and not shown in Figure 8. Figures 9a–9c show site locations. Figure 9d shows mean Δ CMC time series for numbered clusters.

are similar to the case occurred at a few stations in Mammoth Lake, California, where the atmosphere and local topography are found to be responsible for such a phenomenon [Materna and Herring, 2013].

2. The twentieth cluster represents large arc-like motion since 2009 in three distinct regions in California: the region along the California Aqueduct in Mendota city (site P300), Oxnard (site VNCO), and the Bradbury Dam

of Lake Cachuma (site BBDM). Those locations may be sensitive to the change of the surface/underground water.

3. There are several cases of large position scatters for stations in local areas, e.g., near the Augustine volcano (the sixteenth cluster) and the Pogromni volcano (the 24th cluster) in Alaska, which might be related to volcanic activities.

More assessments of the origins of the clusters are presented in Table A1 in Appendix A.

6. Discussions

6.1. CMC and Seasonal Variation of Station Positions

It is well known that there are seasonal (mostly annual and semiannual) variations in CGPS station position time series, especially in the vertical direction. The seasonal terms are usually modeled as sinusoids irrespective of their physical origins when estimating the linear rate of station movement. The seasonal motion is also one kind of CMC, because most of them are of geophysical origins, e.g., the surface and subsurface mass redistributions. However, we prefer to remove them before doing the spatial filtering of CMC because for a regional network, the CMCs are usually spatially homogeneous, but the annual terms may not be; estimation of the CMCs could be compromised by the annual terms if the annual terms are not eliminated first. Figure S4 in the supporting information shows the annual terms for the north, east, and vertical components, respectively. There are large differences for annuals in several adjacent regions; i.e., the annual motions of CGPS stations are not spatially homogeneous. This is the consequence of the fact that geophysical loading can vary greatly over relatively short distance. For example, the phases of the east and vertical annual terms almost flip for a few stations on the two sides of Sierra Nevada Mountains [Amos *et al.*, 2014]. On the basis of the above consideration we find that better filtering results will be obtained if the annual terms are estimated and removed prior to the application of the CMC filtering.

6.2. Comparison Between CWSF and PCA Methods

Although both our CWSF and the PCA methods work for filtering of residual CGPS station position time series, their approaches are fundamentally different. The PCA method performs principal component analysis of the daily position residuals and carries out the filtering by removing the top ranking components which show the most common spatial correlations. The CWSF method, on the other hand, relies on correlations of individual station pairs acquired in the past time series, with no requirement of current correlation information of the sites. Using the PCA method, one could, in principle, keep improving the filtering with less RMS of the post-filtering residuals as long as more principal components are being filtered out, at the price of adding more degree of freedom into the filter. The CWSF method, however, does not really have free parameters to play with as long as it is tuned using past residual time series data.

6.3. Searching for Origin of CMC: Effect of Station Elevation

Some parts of regional common movements in CGPS positions are suggested to be caused by imperfect error modeling during GPS data processing; e.g., the tropospheric delay modeling is affected by both meteorological condition and elevation of the observation made. Because our target study region covers very diverse topography where data processing errors are expected to vary, possibly associated with elevation, we examine whether the elevation difference of CGPS stations could play a role in shaping the common-mode signals observed by CGPS sites. We use a stacked correlation map to investigate the relationship: we first calculate correlations among all the possible station pairs and categorize the results into a grid based on station horizontal (X axis) and vertical (Y axis) separation distances for specific cell size, e.g., 50 km (baseline length) \times 50 m (elevation difference). The correlations falling into each pixel is then averaged. In order to exclude the effect of site-specific and regional transients, we use the interstation correlation results derived using Group II sites which are usually free from major anomalies as discussed in section 3. The resulting correlation plots of horizontal separation versus elevation difference do show a statistical trend of decrease with the increase of station elevation difference within relatively short baseline range (e.g., <200 km). The effect is no longer significant for baseline range greater than 400 km. The case for the north component is shown in Figure 10, and the east and vertical components show similar variations (Figures S5 and S6 in the supporting information). Such a correlation variation confirms that topography is an affecting factor that could result in scatter similarity (i.e., nontectonic common-mode noises) of CGPS positions.

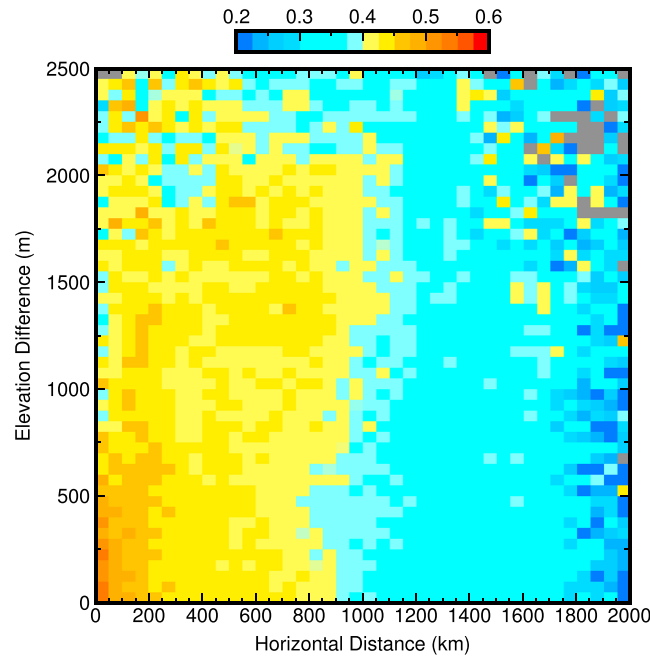


Figure 10. Stacked correlations of the north component for Group II WNAM CGPS sites. The X axis denotes the great circle distance between two CGPS stations; the Y axis denotes the station elevation difference. The grid cells are 50 km × 50 m in size.

6.4. Characteristics of the Correlation-Based Clustering Technique

When presenting the clustering results in section 5.2.2, we use a correlative distance threshold $c=0.3$ to cut the hierarchical clustering tree to form groups that are affected by certain transients. However, this parameter can be adjusted to extract clusters correlated at different levels. For example, a smaller correlative distance threshold will yield clusters at a higher correlation level. The case for $c=0.2$ is presented in Figure 11, showing that only sites with strong correlations are grouped together. The three (first, third, and seventh) clusters in Figure 11 represent the ETS sequence in Cascadia with slight regional differences, which are combined and expanded to become the second cluster in Figure 8. The same situations occur for the other clusters in Figure 11. For example, the second, fourth, and ninth clusters in Figure 11 correspond to the expanded fourth, sixth, and seventh clusters in Figure 8, respectively.

Alternatively, a more comprehensive way to explore the regional transient is to examine the hierarchical clustering tree itself from which we can learn exactly how sites are linked together. The analysis and identification of transient signals can be accomplished in an effective way with the help of graphical user interface which includes the clustering tree, time series, and site map.

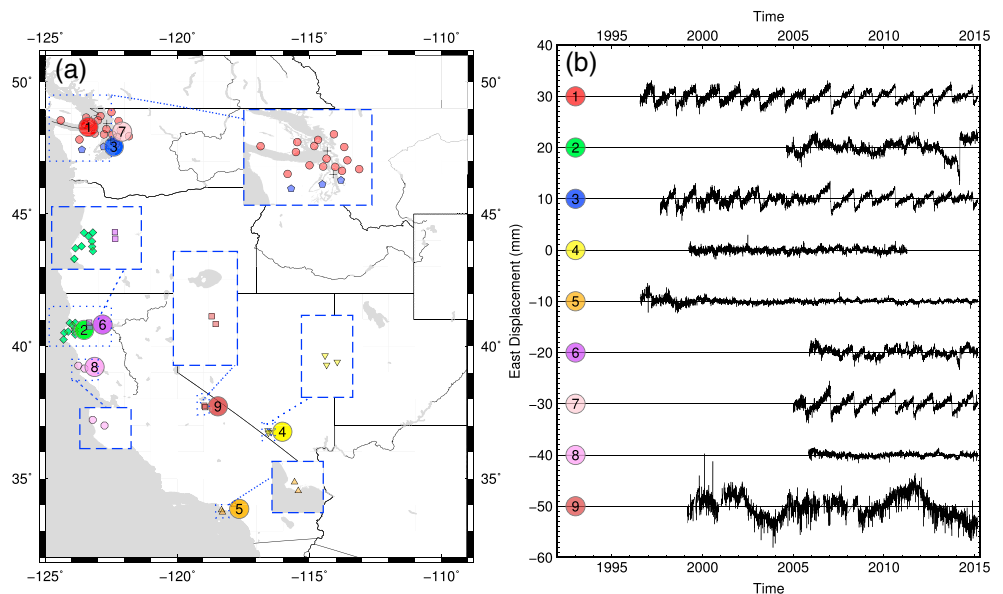


Figure 11. Same as Figure 8, but for cutting correlative distance of $c = 0.2$. Only the first nine clusters (ordered by number of members) are shown.

7. Conclusions

We develop a correlation-weighted spatial filtering algorithm, to extract coherent signals from a dense CGPS network. The new filter is similar to regional stacking technique developed in previous studies [e.g., Nikolaidis, 2002; Márquez-Azúa and Demets, 2003] but different in several important aspects, enabling us to achieve better filtering results and detect more subtle tectonic deformation signals. We have successfully applied our method to the WNAM CGPS station position time series produced by SOPAC and obtained the following results:

1. CME (the large-scale CMC) is found not spatially homogenous. With the increase of site separation, the similarity between CME decreases nearly linearly. The slopes of the distance-correlation relations, however, may vary in different geographic areas. Therefore, when calculating CMC, the weighting scheme using the interstation correlation derived from past residual position time series makes the new filter adapt better the spatial characteristics of CMCs than the traditional stacking methods which assume a homogenous CME or a simple piecewise linear distance-correlation variation, and our method is thus more reasonable and effective.
2. The selection of sites used to derive CMC is not predetermined, but based on evaluation of a weighting scheme including correlation and distance. The optimal selection of sites and their weights is carried out objectively through a grid search which derives the CMC that minimizes the RMS of the filtered residual position time series, excluding any human intervention.
3. The new filter can remove any signals that are common to a subset of CGPS stations from position time series regardless of the origins. By varying distance thresholds, CMC of certain spatial scale can be extracted, whose pattern can be episodic (transient), periodic (seasonal), or decadal (postseismic). Using a hierarchical clustering algorithm, various small-scale transient signals can be effectively identified based upon differencing CMC time series which contain only regional transient signals. Application of the method to the WNAM CGPS network has indeed discovered more coherent transient deformations than those previously known. Some of the transient signals are related to tectonic and volcanic activities (e.g., ETS). A detailed analysis on origin of each transient signal is beyond the scope of this paper.
4. A portion of CMC is proved to be correlated with the elevation of GPS station location. The most likely mechanism is the imperfection of error modeling during GPS data processing. The elevation-dependent residuals may contain contributions from tropospheric delays and/or the mass loading effects.

We so far only tested the new CMC filter for the WNAM CGPS network, but it can be used for other networks to detect and/or remove the CMC signals that are common to more than one sites. The extraction of CMC will benefit the study of its physical origins by analyzing the spatial-temporal characteristics.

Appendix A: Regional Transient Clusters for WNAM East Component

We here present Table A1, the clustering member sites list and the candidate origins for the regional transient signals detected in the east component time series of the WNAM CGPS stations. Detailed analysis on the origins for the 1–7 clusters is presented in section 5.2.2. For geographic locations of the CGPS sites in the table, the readers may refer to the websites of PBO (<http://www.unavco.org/instrumentation/networks/status/pbo>) and SOPAC (<http://sopac.ucsd.edu/>).

Table A1. Regional Transient Signals in the East Component for WNAM CGPS Network

No	Sites#	Cluster Member Sites	Locations	Origins of Transient Signals
1	55	AOA1 BSRY CAT2 CBHS CHIL CIRX CLAR COPR CRU1 CSN1 CSST CTDM ECFS ESRE EWPP FMVT FVPK HOLP HVYS JPLM LAPC LEEP LFRS LINJ LL01 LORS MAT2 MIG1 MLFP MPWD NHRG P606 PMHS PPBF PVE3 PVEP PVRS RHCL ROCK RSVY RTHS SBCC SCIA SFDM SPK1 SPMS SRS1 TORP TRAK UCLP USC1 VNCX VTIS WKPK WMAP	Southern California	(a) Logarithmic-like postseismic decays following the 1994 $M6.7$ Northridge earthquake, the 1999 $M7.1$ Hector Mine earthquake, and the 2010 $M_w7.2$ El Mayor-Cucapah earthquake (only at a portion of stations); (b) larger scatters in the 1990s; and (c) one nontectonic jump on 17 April 2011.

Table A1. (continued)

No	Sites#	Cluster Member Sites	Locations	Origins of Transient Signals
2	49	ALBH ARLI BAMF CHCM CHWK CLRS COUP ELSR GLDR KTBW LKCP LNGB LSIG NANO NEAH NTKA P399 P400 P401 P402 P418 P419 P423 P424 P426 P430 P435 P436 P437 P438 P439 P440 P441 P442 PABH PFLD PGC5 PRDY PTRF PUPU RPT1 SC02 SC03 SC04 SEAI SEAT SEDR THUN WHD1	Northern Cascadia	ETS.
3	45	CHZZ CPXX CVO1 JIME JRO1 MCSO P367 P374 P376 P395 P396 P397 P398 P404 P405 P406 P407 P408 P409 P410 P411 P412 P414 P417 P420 P421 P425 P427 P429 P431 P432 P446 P689 P691 P694 P698 P700 P701 P702 P705 STAY TPW2 TWHL WDBN YELM	Central Cascadia	ETS.
4	15	P058 P157 P158 P159 P160 P164 P165 P166 P167 P168 P169 P170 P274 P324 P326	Southern Cascadia (MTJ region)	Seismic displacements caused by several offshore earthquakes: (a) the 2005 M_w 7.2, (b) the 2010 M 6.5, and (c) the 2014 M_w 6.8 events.
5	11	P181 P210 P211 P212 P229 P255 P257 P275 P276 P306 P534	Central California	Subtle transient signals.
6	10	BEAT BULL BUST CRAT LITT PERL RELA REPO STRI TATE	Beatty, Nevada	Subtle transient signals.
7	9	BKR1 DDMN KNOL LINC P203 P634 P635 PMTN SAWC	Long Valley Caldera, California	Volcanic activities.
8	6	CHO1 P156 P314 P315 P322 P339	Northern California	Same as the fourth cluster.
9	6	P059 P185 P186 P189 P312 P313	Northern California	Same as the fourth cluster.
10	5	BKAP HCMN PHLB RAMT THCP	Southern California	Weak residual postseismic displacements following the 4 April 2010 M_w 7.2 El Mayor-Cucapah earthquake at Baja California.
11	4	BMHL CTMS OPBL OPCX	Southern California	(a) Residual postseismic displacements following the 16 October 1999 M_w 7.1 Hector Mine earthquake; (b) a possible rate change induced by 28 September 2004 M_w 6.0 Parkfield earthquake; and (c) residual seismic displacements induced by the 4 April 2010 M_w 7.2 El Mayor-Cucapah earthquake at Baja California.
12	4	P182 P196 P208 P270	Northern California	Subtle transient signals.
13	4	P330 P332 P338 P341	Northern California	(a) ETS; (b) seismic jumps by the 10 January 2010 M 6.5 and the 10 March 2014 M_w 6.8 earthquakes (same as the two events for the fourth cluster).
14	4	DSME P473 P474 P478	Southern California	Same as the tenth cluster.
15	4	P281 P282 P296 P298	Central California	A few large scatters.
16	4	AV02 AV18 AV19 AV20	Augustine volcano, Alaska	Large scatters with unconfirmed reasons (possibly related to volcanic activities).
17	4	CHAB P253 P256 TIBB	Central California	(a) Large scatters resulting from poor realization of reference frame in the 1990s; (b) unknown irregular seasonal signals and small jumps.
18	3	REP2 REP3 REP4	Nye County, Nevada	Subtle transient signals (colocated sites with only about 2 year continuous observations).
19	3	GVR5 OXYC VDCY	Southern California	Same as the first cluster, but only the 1999 and 2010 events are observable.
20	3	BBDM P300 VNCO	Southern California	Different locations but with similar large arc-like motions possibly related to underground water change.
21	3	I40A LDES LDSW	Southern California	Subtle transient signals.
22	3	P280 P290 P294	Central California	Subtle transient signals.

Table A1. (continued)

No	Sites#	Cluster Member Sites	Locations	Origins of Transient Signals
23	3	P283 P541 P547	Central California	Subtle transient signals.
24	2	AV24 AV25	Pogromni volcano, Unimak Island, Alaska	Nonlinear motions and large scatters possibly related to volcano activities or local climate conditions.
25	2	AC62 AC77	Denali fault, Alaska	Postseismic deformations following the 3 November 2002 M_w 7.9 Denali earthquake.
26	2	MVFD NSSS	Southern California	Same as the tenth cluster.
27	2	HOGS MASW	Parkfield, California	Residual postseismic displacements following the 28 September 2004 $M_6.0$ Parkfield earthquake.
28	2	P287 P297	Central California	Subtle transient signals.
29	2	P327 P793	Northern California	Same as the thirteenth cluster.
30	2	MFTN MFTS	Boulder, Colorado	Large scatters (collated sites adjacent to MFPO and MFTS; out the range of Figure 9).
31	2	P094 P726	Central California	Subtle transient signals.
32	2	P331 P343	Northern California	Same as the thirteenth cluster.
33	2	AV06 MSWB	Akutan Island, Alaska	A transient signal that occurred during the first half of 2008 [Ji and Herring, 2011] and large scatters.
34	2	P214 P234	Central California	Subtle transient signals.
35	2	P061 P371	Northern Cascadia	ETS.
36	2	P248 UCSF	Central California	Subtle transient signals.
37	2	P637 P654	Mono lake, California	Skewed scatters.
38	2	P161 P162	Northern California	Subtle transient signals.
39	2	P569 P580	Searles Lake, California	Skewed scatters.
40	2	AC36 AC43	Kenai Peninsula, Alaska	High-frequency position shifts.
41	2	CRBT MEE2	Central California	Small position jumps.
42	2	P811 P812	California City, California	Collocated sites with large scatters.
43	2	P487 P504	Salton Sea, California	Subtle transient signals.
44	2	P329 P345	Northern California	Same as the thirteenth cluster.
45	2	P809 P810	Delano, California	High-frequency seasonal motions and larger scatters, possibly resulting from seasonal hydrological variations.

Acknowledgments

We thank Roland Bürgmann, Peng Fang, Min Wang, and Ruiqi Li for their constructive comments. We are also grateful to Editor Tregoning, the Associate Editor, and two anonymous reviewers for their comments and suggestions that helped improve the manuscript substantially. We thank SOPAC for making the WNAM CGPS position time series publicly available. The time series data used in this paper are available at the SOPAC website <http://garner.ucsd.edu/pub/timeseries/measures/ats/>. The unfiltered residual position time series data (WesternNorthAmerica/WNAM_Clean_ResidNeuTimeSeries_comb_20150318.tar) and the PCA-filtered position time series data (WesternNorthAmerica/WNAM_Filter_ResidNeuTimeSeries_comb_20150318.tar) were produced on 18 March 2015 and last accessed on 24 March 2015. The code used in this paper is developed in Interactive Data Language (IDL) from the Exelis Inc. (<http://www.exelisis.com>). The code is

References

- Amos, C. B., P. Audet, W. C. Hammond, R. Bürgmann, I. A. Johanson, and G. Blewitt (2014), Uplift and seismicity driven by groundwater depletion in central California, *Nature*, *509*, 483–486, doi:10.1038/nature13275.
- Argus, D. F., M. B. Heflin, G. Peltzer, F. Crampé, and F. H. Webb (2005), Interseismic strain accumulation and anthropogenic motion in metropolitan Los Angeles, *J. Geophys. Res.*, *110*, B04401, doi:10.1029/2003JB002934.
- Barbot, S., Y. Fialko, and Y. Bock (2009), Postseismic deformation due to the M_w 6.0 2004 Parkfield earthquake: Stress-driven creep on a fault with spatially variable rate-and-state friction parameters, *J. Geophys. Res.*, *114*, B07405, doi:10.1029/2008JB005748.
- Blewitt, G., C. Kreemer, W. C. Hammond, and J. M. Goldfarb (2013), Terrestrial reference frame NA12 for crustal deformation studies in North America, *J. Geodyn.*, *72*, 11–24, doi:10.1016/j.jjog.2013.08.004.
- Borsa, A. A., D. C. Agnew, and D. R. Cayan (2014), Ongoing drought-induced uplift in the western United States, *Science*, *345*(6204), 1587–1590, doi:10.1126/science.1260279.
- Brooks, B., J. Foster, D. Sandwell, C. Wolfe, P. Okubo, M. Poland, and D. Myer (2008), Magmatically triggered slow slip at Kilauea Volcano, Hawaii, *Science*, *321*(5893), 1177, doi:10.1126/science.1159007.
- Calais, E., J. Y. Han, C. DeMets, and J. M. Nocquet (2006), Deformation of the North American plate interior from a decade of continuous GPS measurements, *J. Geophys. Res.*, *111*, B06402, doi:10.1029/2005JB004253.
- de Hoon, M. J. L., S. Imoto, J. Nolan, and S. Miyano (2004), Open source clustering software, *Bioinformatics*, *20*(9), 1453–1454, doi:10.1093/bioinformatics/bth078.
- Dong, D., P. Fang, Y. Bock, M. K. Cheng, and S. Miyazaki (2002), Anatomy of apparent seasonal variations from GPS-derived site position time series, *J. Geophys. Res.*, *107*(B4), 2075, doi:10.1029/2001JB000573.
- Dong, D., P. Fang, Y. Bock, F. Webb, L. Prawirodirdjo, S. Kedar, and P. Jamason (2006), Spatiotemporal filtering using principal component analysis and Karhunen-Loeve expansion approaches for regional GPS network analysis, *J. Geophys. Res.*, *111*, B03405, doi:10.1029/2005JB003806.
- Dragert, H., K. Wang, and T. S. James (2001), A silent slip event on the deeper Cascadia subduction interface, *Science*, *292*(5521), 1525–1528, doi:10.1126/science.1060152.
- Freed, A. M., R. Bürgmann, E. Calais, J. Freymueller, and S. Hreinsdóttir (2006), Implications of deformation following the 2002 Denali, Alaska, earthquake for postseismic relaxation processes and lithospheric rheology, *J. Geophys. Res.*, *111*, B01401, doi:10.1029/2005JB003894.
- Fu, Y., and J. T. Freymueller (2013), Repeated large slow slip events at the south central Alaska subduction zone, *Earth Planet. Sci. Lett.*, *375*, 303–311, doi:10.1016/j.epsl.2013.05.049.

incorporated into the iGPS tool package for GPS position time series analysis and available from the GPS Toolbox collection (<http://www.ngs.noaa.gov/gps-toolbox>). The figures were created using the Generic Mapping Tools (GMT) [Wessel and Smith, 1995]. This work was jointly supported by grants from the National Science Foundation of China (41104001 and 41090294), Institute of Crustal Dynamics, China Earthquake Administration (ZDJ2013-22), and by a National Science Foundation (NSF) I/RD grant (EAR-1323052) for the corresponding author as a rotator program director at NSF. Any opinion, findings, and conclusions or recommendations expressed in this material are those of the author(s) and do not necessarily reflect the views of NSF.

- Heki, K., and T. Kataoka (2008), On the biannually repeating slow-slip events at the Ryukyu Trench, southwestern Japan, *J. Geophys. Res.*, *113*, B11402, doi:10.1029/2008JB005739.
- Holtkamp, S., and M. R. Brudzinski (2010), Determination of slow slip episodes and strain accumulation along the Cascadia margin, *J. Geophys. Res.*, *115*, B00A17, doi:10.1029/2008JB006058.
- Ji, K. H., and T. A. Herring (2011), Transient signal detection using GPS measurements: Transient inflation at Akutan volcano, Alaska, during early 2008, *Geophys. Res. Lett.*, *38*, L06307, doi:10.1029/2011GL046904.
- Ji, K. H., and T. A. Herring (2012), Correlation between changes in groundwater levels and surface deformation from GPS measurements in the San Gabriel Valley, California, *Geophys. Res. Lett.*, *39*, L01301, doi:10.1029/2011GL050195.
- Ji, K. H., T. A. Herring, and A. L. Llenos (2013), Near real-time monitoring of volcanic surface deformation from GPS measurements at Long Valley Caldera, California, *Geophys. Res. Lett.*, *40*, 1054–1058, doi:10.1002/grl.50258.
- Jiang, Y., S. Wdowinski, T. H. Dixon, M. Hackl, M. Protti, and V. Gonzalez (2012), Slow slip events in Costa Rica detected by continuous GPS observations, 2002–2011, *Geochem. Geophys. Geosyst.*, *13*, Q04006, doi:10.1029/2012GC004058.
- Khan, S. A., J. Wahr, E. Leuliette, T. van Dam, K. M. Larson, and O. Francis (2008), Geodetic measurements of postglacial adjustments in Greenland, *J. Geophys. Res.*, *113*, B02402, doi:10.1029/2007JB004956.
- King, N. E., et al. (2007), Space geodetic observation of expansion of the San Gabriel Valley, California, aquifer system, during heavy rainfall in winter 2004–2005, *J. Geophys. Res.*, *112*, B03409, doi:10.1029/2006JB004448.
- Kogan, M. G., and G. M. Steblov (2008), Current global plate kinematics from GPS (1995–2007) with the plate-consistent reference frame, *J. Geophys. Res.*, *113*, B04416, doi:10.1029/2007JB005353.
- Larson, K. M., M. Poland, and A. Miklius (2010), Volcano monitoring using GPS: Developing data analysis strategies based on the June 2007 Kilauea Volcano intrusion and eruption, *J. Geophys. Res.*, *115*, B07406, doi:10.1029/2009JB007022.
- Lin, K.-C., J.-C. Hu, K.-E. Ching, J. Angelier, R.-J. Rau, S.-B. Yu, C.-H. Tsai, T.-C. Shin, and M.-H. Huang (2010), GPS crustal deformation, strain rate, and seismic activity after the 1999 Chi-Chi earthquake in Taiwan, *J. Geophys. Res.*, *115*, B07404, doi:10.1029/2009JB006417.
- Lin, L. I.-K. (1989), A concordance correlation coefficient to evaluate reproducibility, *Biometrics*, *45*(1), 255–268.
- Lin, L. I.-K. (2000), Correction: A note on the concordance correlation coefficient, *Biometrics*, *56*(1), 324–325.
- Márquez-Azúa, B., and C. DeMets (2003), Crustal velocity field of Mexico from continuous GPS measurements, 1993 to June 2001: Implications for the neotectonics of Mexico, *J. Geophys. Res.*, *108*(B9), 2450, doi:10.1029/2002JB002241.
- Marshall, S. T., G. J. Funning, and S. E. Owen (2013), Fault slip rates and interseismic deformation in the western Transverse Ranges, California, *J. Geophys. Res. Solid Earth*, *118*, 4511–4534, doi:10.1002/jgrb.50312.
- Materna, K., and T. Herring (2013), Analysis of skewed GPS position estimates: Effects of coupling local topography and atmospheric conditions, Abstract G53A-0907 presented at AGU Fall Meeting 2013, San Francisco, Calif.
- Mazzotti, S., H. Dragert, J. Henton, M. Schmidt, R. Hyndman, T. James, Y. Lu, and M. Craymer (2003), Current tectonics of northern Cascadia from a decade of GPS measurements, *J. Geophys. Res.*, *108*(B12), 2554, doi:10.1029/2003JB002653.
- Meade, B. J., and B. H. Hager (2005), Block models of crustal motion in southern California constrained by GPS measurements, *J. Geophys. Res.*, *110*, B03403, doi:10.1029/2004JB003209.
- Melbourne, T. I., F. H. Webb, J. M. Stock, and C. Reigber (2002), Rapid postseismic transients in subduction zones from continuous GPS, *J. Geophys. Res.*, *107*(B10), 2241, doi:10.1029/2001JB000555.
- Melbourne, T. I., W. M. Szeliga, M. M. Miller, and V. M. Santillan (2005), Extent and duration of the 2003 Cascadia slow earthquake, *Geophys. Res. Lett.*, *32*, L04301, doi:10.1029/2004GL021790.
- Nikolaidis, R. (2002), Observation of geodetic and seismic deformation with the Global Positioning System, PhD thesis, Univ. of Calif., San Diego.
- Prawirodirdjo, L., and Y. Bock (2004), Instantaneous global plate motion model from 12 years of continuous GPS observations, *J. Geophys. Res.*, *109*, B08405, doi:10.1029/2003JB002944.
- Ray, J., Z. Altamimi, X. Collilieux, and T. van Dam (2008), Anomalous harmonics in the spectra of GPS position estimates, *GPS Solut.*, *12*, 55–64, doi:10.1007/s10291-007-0067-7.
- Savage, J. C., and J. Langbein (2008), Postearthquake relaxation after the 2004 M6 Parkfield, California, earthquake and rate-and-state friction, *J. Geophys. Res.*, *113*, B10407, doi:10.1029/2008JB005723.
- Savage, J. C., and R. W. Simpson (2013), Clustering of velocities in a GPS network spanning the Sierra Nevada Block, the Northern Walker Lane Belt, and the Central Nevada Seismic Belt, California-Nevada, *J. Geophys. Res. Solid Earth*, *118*, 4937–4947, doi:10.1002/jgrb.50340.
- Savage, J. C., and J. L. Svarc (2009), Postseismic relaxation following the 1992 M7.3 Landers and 1999 M7.1 Hector Mine earthquakes, southern California, *J. Geophys. Res.*, *114*, B01401, doi:10.1029/2008JB005938.
- Schmalzle, G. M., R. McCaffrey, and K. C. Creager (2014), Central Cascadia subduction zone creep, *Geochem. Geophys. Geosyst.*, *15*, 1515–1532, doi:10.1002/2013GC005172.
- Sella, G. F., S. Stein, T. H. Dixon, M. Craymer, T. S. James, S. Mazzotti, and R. K. Dokka (2007), Observation of glacial isostatic adjustment in “stable” North America with GPS, *Geophys. Res. Lett.*, *34*, L02306, doi:10.1029/2006GL027081.
- Shen, Z.-K., R. W. King, D. C. Agnew, M. Wang, T. A. Herring, D. Dong, and P. Fang (2011), A unified analysis of crustal motion in Southern California, 1970–2004: The SCEC crustal motion map, *J. Geophys. Res.*, *116*, B11402, doi:10.1029/2011JB008549.
- Simpson, R. W., W. Thatcher, and J. C. Savage (2012), Using cluster analysis to organize and explore regional GPS velocities, *Geophys. Res. Lett.*, *39*, L18307, doi:10.1029/2012GL052755.
- Szeliga, W., T. I. Melbourne, M. M. Miller, and V. M. Santillan (2004), Southern Cascadia episodic slow earthquakes, *Geophys. Res. Lett.*, *31*, L16602, doi:10.1029/2004GL020824.
- Takayama, H., and A. Yoshida (2007), Crustal deformation in Kyushu derived from GEONET data, *J. Geophys. Res.*, *112*, B06413, doi:10.1029/2006JB004690.
- Tregoning, P., and T. van Dam (2005), Atmospheric pressure loading corrections applied to GPS data at the observation level, *Geophys. Res. Lett.*, *32*, L22310, doi:10.1029/2005GL024104.
- vanDam, T. M., G. Blewitt, and M. B. Heflin (1994), Atmospheric pressure loading effects on Global Positioning System coordinate determinations, *J. Geophys. Res.*, *99*(B12), 23,939–23,950, doi:10.1029/94JB02122.
- Wdowinski, S., Y. Bock, J. Zhang, P. Fang, and J. Genrich (1997), Southern California permanent GPS geodetic array: Spatial filtering of daily positions for estimating coseismic and postseismic displacements induced by the 1992 Landers earthquake, *J. Geophys. Res.*, *102*(B8), 18,057–18,070, doi:10.1029/97JB01378.
- Webb, F. H., M. Bursik, T. Dixon, F. Farina, G. Marshall, and R. S. Stein (1995), Inflation of Long Valley Caldera from one year of continuous GPS observations, *Geophys. Res. Lett.*, *22*(3), 195–198, doi:10.1029/94GL02968.
- Wech, A. G., K. C. Creager, and T. I. Melbourne (2009), Seismic and geodetic constraints on Cascadia slow slip, *J. Geophys. Res.*, *114*, B10316, doi:10.1029/2008JB006090.

- Wei, M., and J. J. McGuire (2014), The M_w 6.5 offshore Northern California earthquake of 10 January 2010: Ordinary stress drop on a high-strength fault, *Geophys. Res. Lett.*, *41*, 6367–6373, doi:10.1002/2014GL061043.
- Wessel, P., and W. H. F. Smith (1995), New version of the generic mapping tools released, *Eos Trans. AGU*, *76*(33), 329, doi:10.1029/95EO00198.
- William, H. P., A. T. Saul, T. V. William, and P. F. Brian (1992), *Numerical Recipes in C: The Art of Scientific Computing*, 2nd ed., Cambridge Univ. Press, New York.
- Williams, S. D. P., Y. Bock, P. Fang, P. Jamason, R. M. Nikolaidis, L. Prawirodirdjo, M. Miller, and D. J. Johnson (2004), Error analysis of continuous GPS time series, *J. Geophys. Res.*, *109*, B03412, doi:10.1029/2003JB002741.
- Zhang, J., Y. Bock, H. Johnson, P. Fang, S. Williams, J. Genrich, S. Wdowinski, and J. Behr (1997), Southern California permanent GPS geodetic array: Error analysis of daily position estimates and site velocities, *J. Geophys. Res.*, *102*(B8), 18,035–18,055, doi:10.1029/97JB01380.